AGU PUBLICATIONS

Geophysical Research Letters

RESEARCH LETTER
10.1002/2016GL070425

Key Points:
- Rapid convective cooling is predicted to cause solidification of the Orientale melt sheet in ~10 kyr
- Convection inhibits settling of crystals ~1.5 mm in diameter and smaller, preventing fractional crystallization and differentiation
- Dominant crystal size is predicted to be the primary factor controlling impact melt sheet crystallization and differentiation

Supporting Information:
- Supporting Information S1

Correspondence to:
J. P. Cassanelli,
James_Cassanelli@Brown.edu

Citation:
Cassanelli, J. P., and J. W. Head (2016), Did the Orientale impact melt sheet undergo large-scale igneous differentiation by crystal settling?, *Geophys. Res. Lett.*, *43*, 11,156–11,165, doi:10.1002/2016GL070425.

Received 12 JUL 2016
Accepted 18 OCT 2016
Accepted article online 22 OCT 2016
Published online 8 NOV 2016

Did the Orientale impact melt sheet undergo large-scale igneous differentiation by crystal settling?

James P. Cassanelli[1] and James W. Head[1]

[1]Department of Earth, Environmental, and Planetary Sciences, Brown University, Providence, Rhode Island, USA

Abstract Significant quantities of shock-induced melt are predicted to form during basin-scale impact events and may contribute substantially to compositional variation in the lunar crust through differentiation processes. Knowledge of the evolution of impact melt sheets and the cooling and crystallization processes involved is therefore important to understanding the geology and petrology of the Moon. Here we perform a case study on the Orientale basin and investigate the possibility of differentiation of the impact melt sheet by assessing the thermal and physical processes that drive cooling and crystallization, focusing on crystal settling. Results predict that convective processes within the impact melt sheet enhance cooling and solidification and inhibit settling of crystals ~1.5 mm in diameter and smaller, preventing differentiation at or below this size. Impact melt sheet thickness is predicted to have minimal influence on crystallization history, suggesting that crystal size is the primary factor controlling lunar impact melt sheet differentiation.

1. Introduction

Lessons learned from exploration of the Moon, and the analysis of returned samples, have served as the foundation for our understanding of the formation of terrestrial planetary crusts. Specifically, information gathered from the Moon has allowed for the development of the magma ocean hypothesis for crustal formation [e.g., *Wood*, 1975; *Walker et al.*, 1975; *Warren*, 1985; *Elkins-Tanton et al.*, 2011], suggesting that the earliest crust of a terrestrial body is crystallized [e.g., *Elardo et al.*, 2011] directly from an initially molten state (in which a significant portion, or possibly all, of the body was in a liquid state [*Warren*, 1985]).

Crystallization of the lunar magma ocean [*Nemchin et al.*, 2009] and formation of the primary crust has been followed by over 4 Gyr [*Hartmann*, 1980; *Wilhelms et al.*, 1987; *Head et al.*, 2010] of surface modification processes, predominantly in the form of impacts. Impacts are a powerful erosive agent, modifying the primary crust through fracturing, brecciation, physical mixing, and shock-induced melting [*Melosh*, 1989; *Ivanov et al.*, 2010]. The shock-induced melting caused by basin-scale impact events (i.e., those producing a crater ~300 km in diameter or greater [*Baker et al.*, 2012; *Vaughan et al.*, 2013]) is predicted to generate significant volumes of melt [*Cintala and Grieve*, 1998; *Abramov et al.*, 2012]. Given the concentration of large impacts distributed across the surface of the Moon [*Head et al.*, 2010], this suggests that up to ~5% by volume of the Moon's crust may now be comprised of impact melt products [*Vaughan et al.*, 2013]. Despite the potentially significant contribution of impact melt to the crustal composition of the Moon, the processes involved in impact melt sheet cooling and crystallization are not well understood [*Vaughan et al.*, 2013].

Following the impact event, impact melt collects within the excavated crater [e.g., *Warren et al.*, 1996; *Cintala and Grieve*, 1998] and begins cooling and solidification. Crystallization of the impact melt may then proceed by one of two general end-member scenarios: (1) The melt may undergo differentiation during solidification [*Grieve et al.*, 1991; *Cintala and Grieve*, 1998; *Morrison*, 1998; *Zieg and Marsh*, 2005; *Vaughan et al.*, 2013; *Vaughan and Head*, 2014; *Hurwitz and Kring*, 2014] resulting in a newly developed crustal stratigraphy, or (2) the melt may undergo homogeneous solidification and crystallize in equilibrium [e.g., *Vaughan et al.*, 2013], thus homogenizing the crustal stratigraphy. A critical requirement for igneous differentiation is the ability of nucleated crystals to separate from the impact melt by sinking or flotation driven by density differences.

Here we perform a case study on the lunar Orientale basin to explore the possibility for igneous differentiation of the Orientale impact melt sheet [*Head*, 1974] by assessing the thermal and physical processes driving cooling and crystallization, focusing on crystal settling.

2. Orientale Basin

The Orientale basin is a ~930 km multiring impact basin on the lunar far side [*Head*, 1974]. Orientale is the youngest (~3.7–3.8 Ga) [*Baldwin*, 1974; *Wilhelms et al*., 1987; *Whitten et al*., 2011] and most well-preserved impact structure of its size and contains relatively little mare infill [*Whitten et al*., 2011; *Spudis et al*., 2014], which has allowed for accurate morphometric measurements to be made of the interior impact melt deposit [*Head*, 1974]. The well-preserved nature of the impact basin and the availability of reliable measurements of the impact melt sheet make Orientale an ideal candidate for the investigation of impact melt processes and have motivated the selection of Orientale for the case study presented here. Morphometric measurements suggest that the Orientale impact melt sheet is ~350 km in diameter and had an initial thickness of ~15 km [*Vaughan et al*., 2013], yielding a total initial impact melt volume of $\sim 1.5 \times 10^6$ km^3 [*Vaughan et al*., 2013], in good agreement with theoretical scaling law predictions [*Cintala and Grieve*, 1998; *Abramov et al*., 2012].

3. Cooling Processes

Following the impact event, melt created through shock heating of the target material is collected within the excavated crater [*Warren et al*., 1996; *Cintala and Grieve*, 1998]. In this assessment we adopt the interpretation [*Head*, 1974; *Howard et al*., 1974; *McCauley*, 1977; *Head et al*., 1993; *Spudis*, 2005; *Spudis et al*., 2014] that the Maunder Formation within the Orientale basin represents an exposure of the basin impact melt deposit (for alternate views, see *Melosh et al*. [2013]). This interpretation is based on the unique morphology of the Maunder Formation, which hosts a smooth plains facies near the basin center that grades outward into a rough corrugated facies toward the edge of the central depression [*Head*, 1974]. The smooth plains and rough corrugated facies exhibit varying degrees of cracked and pitted surfaces attributed to cooling and contraction of impact melt [*Head*, 1974; *Howard et al*., 1974; *McCauley*, 1977]. The smooth surface, abundance and size of cracks and depositional distribution of the smooth plains facies have been interpreted to suggest that the smooth plains facies represents relatively pure impact melt deposits [*Head*, 1974; *Howard et al*., 1974; *McCauley*, 1977]. Conversely, the rougher surface and smaller cracks exhibited by the rough corrugated facies have been attributed to a more substantial component of impact debris [*Head*, 1974]. On the basis of these interpretations, we assume that the Orientale impact melt sheet was initially exposed at the lunar surface without a thick superposed layer of fallback ejecta or collapsed material and is comprised of pure impact melt, with little contribution from cooler impact debris.

Under these assumptions, the melt sheet is predicted to initially exist in a completely molten superheated state with a temperature, T_i, of ~2275 K [*O'Keefe and Ahrens*, 1975; *O'Keefe and Ahrens*, 1977; *Melosh*, 1989] and would begin to radiate energy away from the upper surface of the impact melt sheet (Figure S1 in the supporting information). In this analysis, conductive heat loss from the walls and floor of the impact melt sheet has been neglected. This is because heat loss from the base and the walls of the melt sheet occurs purely by conduction, which is far less efficient than the convectively enhanced heat loss from the melt sheet surface. In addition, the material forming the base and walls of the impact melt sheet would also have undergone heating during the impact event that would reduce the thermal gradients with the impact melt, further decreasing the efficiency of the conductive heat loss from these surfaces. The radiative top-down cooling experienced by the melt sheet results in the formation of an unstable upper thermal boundary layer [e.g., *Davaille and Jaupart*, 1993] (Figure S1). At this stage a large temperature gradient would exist across the melt sheet (Figure S1), and the configuration would be characterized by very high Rayleigh numbers (~10^{19}). Under these conditions, vigorous convection would take place in the impact melt sheet interior where a relatively constant temperature, T_m (in K), is maintained [*Davaille and Jaupart*, 1993], with downgoing plumes of cool dense material forming at the base of the upper thermal boundary layer (Figure S1).

The convective cooling of the Orientale impact melt sheet can be estimated with empirically derived relationships which describe the thermal convection processes of terrestrial lava lakes [*Davaille and Jaupart*, 1993] due to the generally analogous geometry and thermal processes. This is because a thick flotation crust, which would alter the system geometry and thermal processes, is not predicted to form in impact melts of the lunar crust and upper mantle [*Vaughan et al*., 2013]. A flotation crust is not predicted to form because before anorthite crystallization begins, the prior crystallization of the more dense mineral species originally contained in these melts would have decreased the melt from an initial density of 2800 kg/m^3 below the level

allowing anorthite flotation [*Vaughan et al.*, 2013]. Therefore, in both lava lakes and impact melt sheets without a thick flotation crust, heat is lost from the convectively cooling magma bodies through a thickening surficial thermal boundary layer (Figure S1) which includes a quenched crust and stagnant lid [*Davaille and Jaupart*, 1993] (though the impact melt sheet will initially exist at a much greater temperature with more vigorous convection and a thinner upper thermal boundary layer, evolving toward conditions more similar to a lava lake as solidification proceeds).

Under this assumption, cooling of the impact melt sheet is governed by the amount of heat, F (in W/m^2), that can be conducted through the thickening upper thermal boundary layer [*Davaille and Jaupart*, 1993] and radiated to space. The heat flux across the upper thermal boundary layer depends critically on the temperature contrast, ΔT_c (in K), within the well-mixed interior (Figure S1) and is given by [*Davaille and Jaupart*, 1993]

$$F = 0.16 k_m \left({}^{\alpha g}/_{\kappa \nu_m} \right)^{1/3} \Delta T_c{}^{4/3} \tag{1}$$

where k_m is the thermal conductivity of the melt sheet interior (assuming a typical approximate value of 3 W/m K for magma), α is the coefficient of thermal expansion (for which we take a typical value of 5×10^{-5} K^{-1} [e.g., *Davaille and Jaupart*, 1993]), g is the gravitational acceleration (1.62 m/s^2 on the Moon), κ is the thermal diffusivity of the melt sheet interior (for which we use a typical value of 1×10^{-6} m^2/s), and ν_m is the kinematic viscosity of the melt sheet interior (m^2/s). The temperature gradient in the well-mixed interior (ΔT_c), which drives convection, has been shown to depend only on the "viscous" temperature scale given by [*Davaille and Jaupart*, 1993]

$$\Delta T_c = 2.24 \left(\frac{\mu(T_m)}{\frac{\mathrm{d}\mu}{\mathrm{d}T}(T_m)} \right) \tag{2}$$

where μ is the dynamic viscosity (Pa s) and T_m is the temperature of the well-mixed interior (K) (Figure S1). We model the temperature-dependent viscosity of the impact melt through the implementation of an empirical relation [*Weill et al.*, 1971], with fluid phase viscosity (in poise) as a function of temperature given by

$$\mathrm{Log}(\mu_f(T_m)) = a + b \left(\frac{10^4}{T_m} \right) \tag{3}$$

where a and b are constants, for which we take average values of −5.02 and 0.98 (respectively) derived from measurements of lunar basalts [*Weill et al.*, 1971]. The viscosity of the fluid-crystal mixture below the liquidus temperature (for which we adopt a value of 1525 K, an approximate average value for rocks of basaltic composition) is modeled using the Einstein-Roscoe relationship [*Einstein*, 1906; *Roscoe*, 1952; *Shaw*, 1969; *Ryerson et al.*, 1988; *Harris and Allen*, 2008]:

$$\mu(\phi) = \mu_f(T_m) \left(1 - {}^{\phi}/_{\phi_{\max}}\right)^{-2.5} \tag{4}$$

where ϕ is the crystal content of the fluid and μ_f is the temperature-dependent viscosity of the fluid phase (as determined from equation (3)). The viscosity of the fluid-crystal mixture can be estimated with this relationship until the solid fraction reaches a maximum value, $\phi_{\max}$, suggested to be 0.6 [e.g., *Marsh*, 1981], at which point the viscosity of the fluid-crystal mixture becomes infinite and the mixture takes on a solid-like behavior [e.g., *Pinkerton and Stevenson*, 1992].

The total heat flux leaving the system, F, is determined with equations 1–4 and then integrated over a small increment of time dt (set to 5×10^{-3} years, equal to half of the time interval beyond which the solution no longer showed variability) and deducted from the total heat energy of the system (assuming a linear distribution of latent heat in the phase change temperature region), H (in J/m^2), given by

$$H = \left(\rho c_p T_m + \rho L\right) z \tag{5}$$

where ρ is the density of the melt (for which we use a predicted value of 2800 kg/m^3 [*Vaughan et al.*, 2013]), c_p is the specific heat capacity of the melt (with a typical value of 1000 J/kg K [e.g., *Davaille and Jaupart*, 1993]), L is the latent heat of fusion (with a value of 4×10^5 J/kg, typical of basaltic magmas), and z (in m) is the thickness of the impact melt sheet.

The updated total heat energy of the system is then used to calculate a new mixed interior temperature (T_m) and total solid fraction of the melt, ϕ (initially set to zero), assuming a linear relationship between the solid

fraction and the temperature between the liquidus (T_L) and solidus (T_S, for which we adopt a value of 1225 K, an average value for rocks of basaltic composition) described by

$$\phi \begin{cases} 0;\ T_m > T_L \\ \dfrac{T_m - T_S}{T_L - T_S};\ T_L > T_m > T_S \\ 1;\ T_S > T_m \end{cases} \tag{6}$$

Finally, updated values of the viscosity (μ) and the temperature gradient driving convection (ΔT_c) are computed, and the system is advanced another time step.

4. Crystallization Processes

On the basis of analogous scale and convective vigor, we adopt a crystallization framework developed by *Martin and Nokes* [1988] for vigorously convecting terrestrial magma chambers to assess the crystallization processes involved in impact melt sheet solidification. In this framework, vigorous convection within the well-mixed interior of the melt sheet holds crystals in suspension and prevents settling. Suspended crystals instead settle at the boundaries of the impact melt system where convective velocities decay to zero. Settled crystals are assumed to accumulate at the base of the system (due to the high aspect ratio of the melt sheet geometry) forming a solid layer that resists reentrainment into the convective interior (Figure S1). As a result, as crystals settle out of suspension, the viscosity of the system is updated at each time step using equation (4) to account for any reduction in the suspended solid fraction of the fluid-crystal mixture phase (Figure S1) due to crystal settling. Additionally, as crystals settle out of suspension and the solid settled layer thickens, the thickness of the fluid-crystal mixture layer is reduced. The reduction in thickness of the fluid-crystal mixture layer is tracked throughout cooling and solidification with the following relationship:

$$z(t + \mathrm{d}t) = z(t) - C_S(t) \cdot z(t) \tag{7}$$

where $z(t + \mathrm{d}t)$ is the thickness (in m) of the fluid-crystal mixture layer at the current time, $z(t)$ is the thickness of the fluid-crystal mixture layer (in m) at the previous time, and $C_S(t)$ is the total settled fraction (determined by the process described in the following).

Crystals contained in suspension settle out at the boundaries over a characteristic residence time [*Martin and Nokes*, 1988] where the time, t_r (in s), required for 99% of the crystals in suspension to settle at the nonconvective boundaries is given by [*Suckale et al.*, 2012]

$$t_r = \log(100) \cdot z / v_s \tag{8}$$

where v_s is the Stoke's settling velocity (m/s). Assuming spherical particles for simplicity, the Stoke's settling velocity is given by

$$v_s = \frac{2\Delta\rho g \left(\frac{D}{2}\right)^2}{9\mu} \tag{9}$$

where $\Delta\rho$ is the density difference between the precipitated crystals and the melt (in kg/m^3) and D is the crystal diameter (in m). In order to assess a scenario of maximum settling efficiency, we assume that crystallization occurs at the maximum density contrast possible for the Orientale impact melt sheet throughout the solidification process by adopting a constant $\Delta\rho$ value of 550 kg/m^3. This value is equal to the density difference between olivine, the densest (3350 kg/m^3) mineral phase crystallizing in the Orientale impact melt sheet, and the impact melt sheet itself (2800 kg/m^3) [*Vaughan et al.*, 2013].

A critical parameter required to estimate settling velocities is the diameter of the crystals nucleated within the melt. Here we do not attempt to directly estimate the crystal size due to large uncertainties in the involved analytical approaches. Instead, we choose to adopt more reliable crystal size values determined from observations of lunar impact melt rock samples. However, impact melt rocks collected from the Moon exhibit considerable variability in crystal sizes and petrologic characteristics [e.g., *Taylor et al.*, 1991]. While terrestrial impact melt rocks are more thoroughly studied [e.g., *Dressler and Reimold*, 2001], with better developed constraints on crystal sizes and petrologic characteristics [e.g., *Grieve et al.*, 1991; *Warren et al.*, 1996; *O'Connell-Cooper and Spray*, 2011], terrestrial impact melt sheets formed and evolved under significantly different conditions (i.e., increased volatile abundance and different cooling and compositional conditions) and may not

be representative of lunar impact melt sheets. Therefore, we do not use the terrestrial impact melt rocks to infer petrologic characteristics of lunar impact melts, but later briefly discuss the implications of our results for the differentiated Manicouagan [*O'Connell-Cooper and Spray*, 2011] and Sudbury [*Grieve et al*., 1991] terrestrial impact melt sheets. Crystal sizes of lunar impact melt rocks range from dominantly fine-grained to fine and medium-grained with coarse clasts, while the petrologic characteristics range in nature from impact glasses to impact melt breccias and clast-poor impact melt rocks [e.g., *Taylor et al*., 1991]. Here we assume that the clast-poor impact melt rocks are most representative of the average petrologic characteristics of lunar impact melt sheets because these rocks are generally coherent, with almost pure igneous textures, and are interpreted to have crystallized directly from molten silicate bodies [*Taylor et al*., 1991]. The clast-poor impact melt rocks are predominantly fine-grained (~0–1 mm in size) [*Taylor et al*., 1991], as are most lunar impact melt rocks [e.g., *Ryder and Bower*, 1977; *Onorato et al*., 1978; *Ryder and Spudis*, 1987; *Dalrymple and Ryder*, 1993; *Whitehead et al*., 2002; *Cohen et al*., 2000; *Cohen et al*., 2005; *Warren et al*., 2005]. Therefore, we adopt a crystal size of 1 mm as a representative average of grain sizes produced within crystalizing lunar impact melt sheets and later explore the effects of variable crystal size to address uncertainties in this estimate.

If the residence time of the suspended crystals is less than the time required to solidify and nucleate additional crystals, all the crystals in suspension will settle out [*Suckale et al*., 2012], and the suspended load will decrease until additional crystals are formed through further cooling. Conversely, if the residence time of the suspended crystals exceeds the time required to solidify and nucleate additional crystals, only a portion of the suspended crystals will settle, and the suspended load will increase as cooling proceeds and additional crystals are formed. The cooling and crystallization processes of the system are solved in a time-marching manner until the suspended crystal content of the fluid-crystal mixture layer reaches the maximum value (0.6), or until the total solid fraction of the system reaches a value of 1, resulting from complete crystallization and settling. Thus, by comparing the time required to solidify (Figure 1a) and nucleate crystals within the impact melt sheet against the residence time of the suspended crystals, the fraction of suspended crystals that are able to settle throughout the cooling process can be derived (Figure 1b) (results are displayed for a range of explored crystal diameters from 0.5 mm to 1 cm in 0.5 mm increments, including the nominal 1 mm diameter). The fraction of crystals able to settle, in conjunction with the total solid fraction of the melt sheet, allows the relative fraction of crystals suspended (Figure 1c) versus the fraction of crystals settled (Figure 1d) throughout the cooling and solidification process to be determined.

5. Results and Discussion

Estimates of the convective cooling and crystallization of the Orientale impact melt sheet (with a nominal crystal diameter of 1 mm as determined in section 4) suggest that cooling and crystallization of the structure occurred rapidly, with solidification of the melt reaching the maximum value of 0.6 (beyond which the melt transitions to solid-like behavior [*Pinkerton and Stevenson*, 1992]) within ~10 kyr (Figure 1a). In the initially superheated state, the impact melt is characterized by low viscosities and vigorous convection. As a result, heat loss in this state is very efficient, rapidly cooling the Orientale impact melt sheet down to the liquidus over a period of ~10 years (represented by the flat portions of the cooling/solidification curves depicted in Figure 1a). This cooling phase has minimal effect on the overall cooling history because it is very rapid relative to the total duration of cooling and has no direct influence on the predicted crystallization history because it occurs before the initiation of crystallization (note the identical cooling behavior of each solidification scenario prior to the start of crystallization at the liquidus shown in Figure 1a).

The rapid convective heat loss that is predicted to occur within the Orientale impact melt sheet produces cooling rates that are substantially more rapid than the residence time of suspended crystals throughout most of the cooling and solidification process, inhibiting crystal settling. Limited crystal settling is only able to occur during the early stages of crystallization when the viscosity of the system is low due to low total crystal content and high temperatures (Figure 1b). However, the cumulative amount of possible settling is minimal, with the settled fraction reaching only ~0.15 by the end of the solidification process (Figure 1d). Substantial crystal settling is effectively prevented throughout the solidification process, until the solid fraction of the crystal-melt mixture reaches the maximum value of 0.6 and undergoes a transition to solid-like behavior. This transition in rheological behavior [*Pinkerton and Stevenson*, 1992] would subdue convection

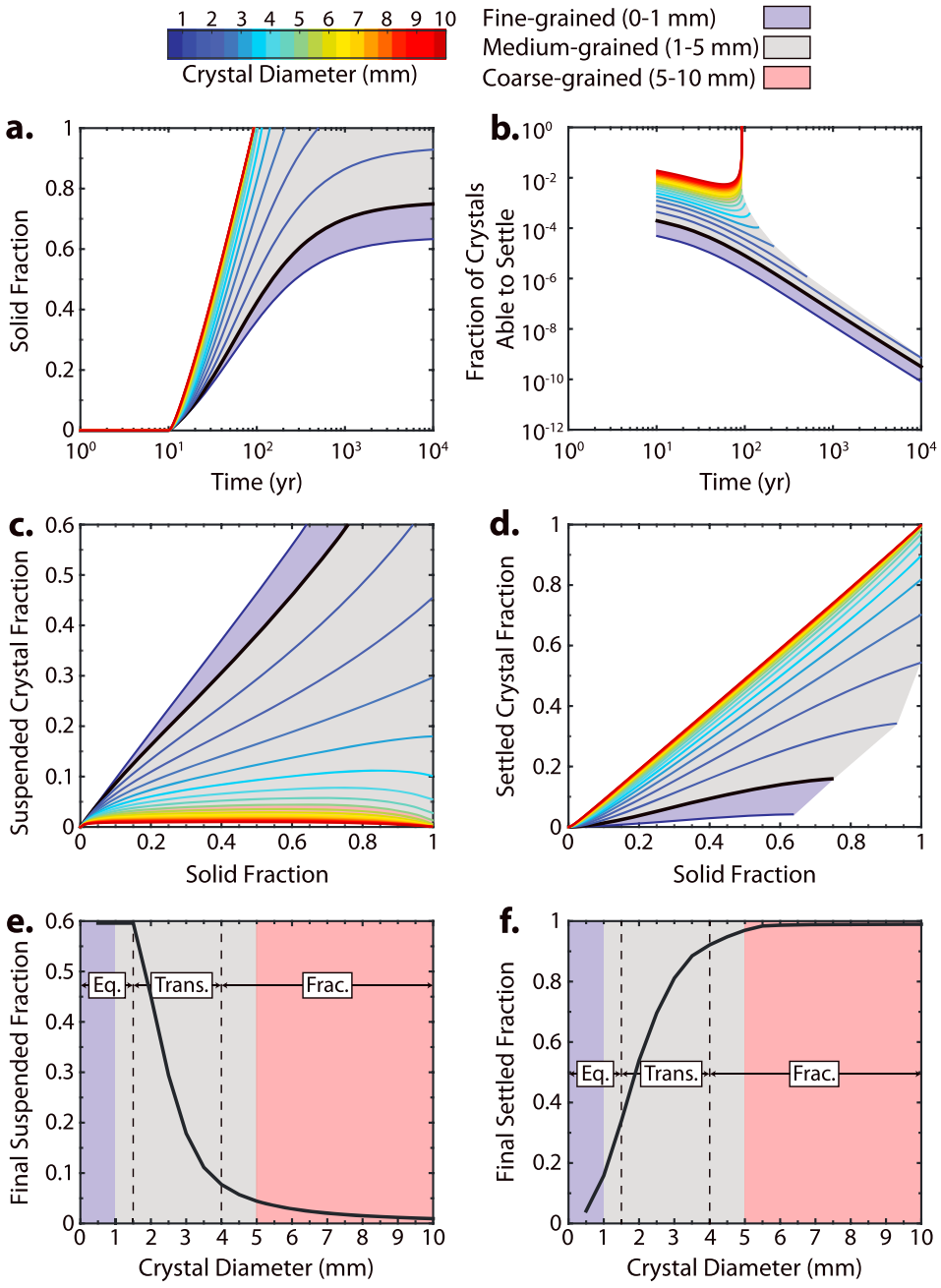

Figure 1. Results of the cooling and crystallization analysis of the ~15 km thick [*Vaughan et al.*, 2013] Orientale impact melt sheet. Figures 1a–1d display model results for a range of crystal diameters from 0.5 mm to 1 cm in 0.5 mm increments with corresponding line colors indicated in the legend. Results for the typical 1 mm crystal diameter adopted for lunar impact melts are displayed by the bold black lines. In all panels, the shaded regions correspond to fine-grained (0–1 mm), medium-grained (1–5 mm), and coarse-grained (5–10 mm) textures as indicated by the legend. (a) The solid fraction of the Orientale impact melt sheet and (b) the fraction of crystals suspended within the melt which are able to settle as a function of time, during the cooling and crystallization process. (c) The fraction of crystals within the Orientale impact melt sheet that remain in suspension and (d) the fraction of crystals that have settled out of suspension at the nonconvective boundaries. Note that as crystal diameter decreases, the fraction of crystals kept in suspension throughout cooling and solidification increases due to inefficient settling, leading to a predicted equilibrium crystallization scenario (where the maximum solid fraction reached is 0.6 as discussed in section 3). In contrast, as crystal diameters increase, more efficient settling causes increased settled fractions and results in a prediction of fractional crystallization. The final (e) suspended and (f) settled crystal fractions reached in the cooling and solidification of the Orientale impact melt sheet as a function of crystal diameter. A sharp transition (Trans.) from equilibrium (Eq.) to fractional (Frac.) crystallization begins at a crystal diameter of ~1.5 mm and completes at a diameter of ~4 mm, as indicated by the dashed lines.

as well as any possible further crystal settling, causing any remaining cooling and crystallization to occur in situ.

The results of this analysis suggest that solid-melt separation through crystal settling is not an efficient process in the convectively cooled Orientale impact melt sheet in the nominal case with 1 mm crystals (Figure 1c and 1d). Therefore, under these conditions, equilibrium crystallization is predicted to dominate during solidification of the Orientale impact melt sheet, and large-scale igneous differentiation is not anticipated. This result is in agreement with petrologic predictions that the Orientale melt sheet underwent equilibrium crystallization [*Vaughan et al.*, 2013]. The results of this analysis suggest that up to ~5% [*Vaughan et al.*, 2013] of the lunar crust may have been homogenized through the shock-induced melting associated with large impacts. While differentiation of the Orientale impact melt deposit is not predicted to have occurred by crystal settling given typical lunar impact melt crystal sizes, the potential for differentiation by other mechanisms, such as viscous emulsion differentiation [*Zieg and Marsh*, 2005], remains.

Additionally, variations in the dominant crystal size and in the scale of the impact melt sheet may alter the cooling rates of the impact melt and the residence time of the crystals within the system and could possibly allow for differentiation. We now explore the effects of both crystal size and melt sheet thickness on the predicted crystallization processes.

6. Crystal Size

The effects of variable crystal size on the cooling and crystallization of the Orientale impact melt sheet are assessed by performing the analysis detailed in sections 3 and 4 for a range of crystal diameters from 0.5 mm to 1 cm in 0.5 mm increments (Figures 1a–1d).

We find that for crystal diameters below ~1.5 mm, long crystal residence times due to low settling velocities result in inefficient crystal settling (Figure 1b). Consequently, for crystal diameters below ~1.5 mm, the predicted suspended crystal fraction (Figure 1c) approaches a line of slope unity when plotted against the total solid fraction of the melt sheet (corresponding to a case in which all increases in the total solid fraction are equaled by increases in the suspended crystal fraction to the maximum suspended fraction of 0.6), while the settled fraction (Figure 1d) approaches a constant value of zero. Therefore, for crystal diameters of ~1.5 mm and less, equilibrium crystallization of the impact melt is predicted as shown in Figures 1e and 1f, which plot the final suspended and settled crystal fractions reached in the cooling and solidification of the Orientale impact melt sheet as a function of crystal diameter.

In contrast, for crystal diameters greater than ~1.5 mm, we find that rapid decreases in residence time owing to greater settling velocities cause increased settling efficiency (Figure 1b) resulting in opposite settling trends relative to the smaller crystal diameters. As crystal diameter increases, the predicted settled crystal fraction (Figure 1d) approaches a line of slope unity when plotted against the total solid fraction of the melt sheet (corresponding to a case in which all increases in the total solid fraction are equaled by increases in the settled crystal fraction), while the suspended fraction (Figure 1c) approaches a constant value of zero. At greater crystal diameters the settled crystal fraction is able to reach unity because the suspended crystal fraction in the crystal-fluid mixture layer never approaches the maximum value of 0.6 (at which point the crystal-melt mixture viscosity trends toward infinity as the mixture transitions to solid-like behavior), thereby allowing crystals to settle and accumulate without the superposed crystal-fluid phase solidifying and preventing further settling. For crystal diameters greater than ~1.5 mm, we find a sharp transition from solidification by equilibrium crystallization to fractional crystallization which completes at a crystal diameter of ~4 mm (Figures 1e and 1f).

Therefore, if the adopted average crystal diameter of 1 mm is representative of the Orientale impact melt sheet, and the dominant crystal diameters formed during the cooling of the impact melt were less than ~1.5 mm, the melt sheet is predicted to have undergone equilibrium crystallization. Conversely, if crystal diameters formed during cooling were greater than ~1.5–4 mm, the Orientale impact melt sheet is predicted to have undergone fractional crystallization and differentiation.

7. The Role of Impact Melt Sheet Thickness

In order to assess the effects of the crater size and impact melt sheet thickness on the predicted cooling and crystallization processes, we investigate the Copernicus impact structure. Copernicus is a ~96 km diameter complex crater located on the lunar near side which hosts evidence for relatively extensive impact melt deposits [*Smrekar and Pieters*, 1985; *Dhingra et al*., 2013]. Impact crater scaling laws [*Cintala and Grieve*, 1998] predict that ~2350 km^3 of melt were generated during the formation of Copernicus. Distributed evenly across the ~58 km diameter floor of Copernicus, this yields an average impact melt deposit thickness of ~220 m (although the assumed even distribution and average depth are likely to have been altered by displacement from the uplifted central peak region). Analysis of a ~220 m thick Copernicus impact melt structure (Figure S2) by the methods outlined in sections 3 and 4 shows no significant differences in the predicted crystallization history (Figures S2c–S2f) versus that of the thicker Orientale impact melt structure (Figures 1c–1f), suggesting that the thickness of the impact melt deposit does not influence the crystallization processes. This is because the effect of more rapid cooling associated with the smaller impact melt structure is counteracted by the reduced residence time of crystals suspended within the impact melt system (because transportation time through the system is reduced as a result of the reduced travel distances), resulting in a neutral net effect. Thus, the limited effect of impact melt thickness indicated by this analysis suggests that the most important factor controlling the crystallization and the potential for igneous differentiation of impact melt systems is the dominant crystal size contained within the melt.

The results of this analysis have interesting implications for the large lunar South Pole Aitken (SPA) basin, which has alternatively been suggested to host a homogeneous [*Pieters et al*., 1997] and differentiated [*Vaughan and Head*, 2014] impact melt sheet. In order for the SPA basin impact melt sheet to have undergone differentiation, our results suggest that the dominant crystal size of the cooling impact melt must have been greater than ~1.5–4 mm in diameter (which could have been facilitated by longer cooling times due to the significant ~50 km thickness of the impact melt structure) [*Vaughan and Head*, 2014].

Additionally, we are currently exploring applications of the concepts developed in this contribution to terrestrial impact melt sheets where considerably different conditions prevailed (i.e., increased volatile abundance and different cooling and compositional conditions). The Sudbury [*Grieve et al*., 1991] and Manicouagan [*O'Connell-Cooper and Spray*, 2011] terrestrial impact melt sheets are both known to have undergone differentiation. Interestingly, the main body of the Sudbury impact melt sheet is coarse-grained [*Grieve et al*., 1991], while the differentiated section of Manicouagan is medium-grained [*O'Connell-Cooper and Spray*, 2011] with fine-grained undifferentiated sections. The differentiation of these impact melt sheets has previously been attributed to their thicknesses [e.g., *O'Connell-Cooper and Spray*, 2011]; however, these observations are also consistent with the predictions of this analysis (Figures 1e and 1f), suggesting instead that the crystal sizes are responsible for the observed differentiation trends.

8. Conclusions

Analysis of the cooling and crystallization processes of the Orientale impact melt sheet indicates that crystals ~1.5 mm in diameter or smaller are not able to efficiently settle out at the boundaries of the convecting melt system. As a result, crystals of this diameter nucleated within the melt remain in suspension, causing the suspended crystal fraction to rise nearly equally with the total melt solid fraction (Figure 1c) until a maximum value of 0.6 is reached after ~10 kyr (Figure 1a). Once the maximum suspended crystal fraction of 0.6 [e.g., *Marsh*, 1981] is reached, the crystal-melt mixture would undergo a rheological transition to solid-like behavior [e.g., *Pinkerton and Stevenson*, 1992], subduing convective and settling motions, and causing any further cooling and crystallization to occur in situ. Therefore, if the estimated average lunar impact melt sheet crystal size of ~1 mm (as determined in section 4) is representative of the Orientale structure, the Orientale impact melt sheet is predicted to have solidified by equilibrium crystallization without large-scale igneous differentiation. Analysis of the effects of variable crystal size indicates that equilibrium crystallization is predicted to occur for crystal diameters smaller than ~1.5 mm (Figures 1e and 1f) due to increased residence times associated with lower settling velocities. In contrast, as crystal diameter increases beyond ~1.5 mm, rapid decreases in residence time due to higher settling velocities allow for increasingly efficient crystal settling throughout the cooling and crystallization of the impact melt sheet (Figures 1c and 1d). As a result, a rapid transition from solidification by equilibrium crystallization to fractional crystallization is predicted within the crystal diameter

range of ~1.5–4 mm (Figures 1e and 1f). Thus, if the crystals formed in the cooling Orientale impact melt sheet were greater in diameter than ~1.5–4 mm, fractional crystallization and large-scale igneous differentiation are predicted. Assessment of the crystallization history of the thinner Copernicus crater impact melt deposits (Figure S2) indicates that impact melt sheet thickness does not significantly influence the crystallization history because the effects of the more rapid cooling are counteracted by the decreased residence times of crystals within the melt system (due to reduced travel distances). Therefore, the results of this analysis suggest that the most important factor controlling the crystallization history of impact melt deposits is the dominant crystal size. The predictions of this analysis are supported by results from petrologic modeling [*Vaughan et al.*, 2013] studies which have also suggested that the Orientale impact melt sheet underwent equilibrium crystallization. If the average crystal size of ~1 mm estimated for the Orientale basin is representative of the other lunar basins, the prediction of equilibrium crystallization suggests that up to ~5% [*Vaughan et al.*, 2013] of the lunar crust may have been compositionally homogenized by the impact melting associated with the large basins distributed across the surface of the Moon.

Acknowledgments

We gratefully acknowledge financial support from the NASA Solar System Exploration Research Virtual Institute (SSERVI) grant for Evolution and Environment of Exploration Destinations (NNA14AB01A), the NASA Lunar Reconnaissance Orbiter (LRO) Mission, Lunar Orbiter Laser Altimeter (LOLA) Experiment Team (grants NNX11AK29G and NNX13AO77G), and the NASA Gravity Recovery and Interior Laboratory (GRAIL) Mission Guest Scientist Program (grant NNX12AL07G). We thank John Spray and Clive R. Neal for constructive reviews which improved the quality of the manuscript. We thank David Weiss and Brandon Johnson for helpful comments and discussion. All data utilized for this paper have been properly cited and referred to in the reference list.

References

Abramov, O., S. M. Wong, and D. A. Kring (2012), Differential melt scaling for oblique impacts on terrestrial planets, *Icarus*, *218*, 906–916, doi:10.1016/j.icarus.2011.12.022.

Baker, D. M. H., J. W. Head, G. A. Neumann, D. E. Smith, and M. T. Zuber (2012), The transition from complex craters to multi-ring basins on the Moon: Quantitative geometric properties from Lunar Reconnaissance Orbiter Lunar Orbiter Laser Altimeter (LOLA) data, *J. Geophys. Res.*, *117*, E00H16, doi:10.1029/2011JE004021.

Baldwin, R. B. (1974), Was there a "terminal lunar cataclysm" 3.9–4.0 $\times 10^9$ years ago?, *Icarus*, *23*, 157–166, doi:10.1016/0019-1035(74)90003-7.

Cintala, M. J., and R. A. F. Grieve (1998), Scaling impact melting and crater dimensions: Implications for the lunar cratering record, *Meteorit. Planet. Sci.*, *33*, 889–912, doi:10.1111/j.1945-5100.1998.tb01695.x.

Cohen, B. A., T. D. Swindle, and D. A. Kring (2000), Support for the lunar cataclysm hypothesis from lunar meteorite impact melt ages, *Science*, *290*, 1754–1756, doi:10.1126/science.290.5497.1754.

Cohen, B. A., T. D. Swindle, and D. A. Kring (2005), Geochemistry and 40Ar-39Ar geochronology of impact-melt clasts in feldspathic lunar meteorites: Implications for lunar bombardment history, *Meteorit. Planet. Sci.*, *40*, 755–777, doi:10.1111/j.1945-5100.2005.tb00978.x.

Dalrymple, G. B., and G. Ryder (1993), 40Ar/39Ar age spectra of Apollo 15 impact melt rocks by laser step-heating and their bearing on the history of lunar basin formation, *J. Geophys. Res.*, *98*, 13,085–13,095, doi:10.1029/93JE01222.

Davaille, A., and C. Jaupart (1993), Thermal convection in lava lakes, *Geophys. Res. Lett.*, *20*, 1827–1830, doi:10.1029/93GL02008.

Dhingra, D., C. M. Pieters, J. W. Head, and P. J. Isaacson (2013), Large mineralogically distinct impact melt feature at Copernicus crater—Evidence for retention of compositional heterogeneity, *Geophys. Res. Lett.*, *40*, 1043–1048, doi:10.1002/grl.50255.

Dressler, B. O., and W. U. Reimold (2001), Terrestrial impact melt rocks and glasses, *Earth Sci. Rev.*, *56*, 205–284, doi:10.1016/S0012-8252(01)00064-2.

Einstein, A. (1906), Eine neue bestimmung der moleküldimensionen, *Ann. Phys.*, *324*, 289–306, doi:10.1002/andp.19063240204.

Elardo, S. M., D. S. Draper, and C. K. Shearer Jr. (2011), Lunar magma ocean crystallization revisited: Bulk composition, early cumulate mineralogy, and the source regions of the highlands Mg-suite, *Geochim. Cosmochim. Acta*, *75*, 3024–3045, doi:10.1016/j.gca.2011.02.033.

Elkins-Tanton, L. T., S. Burgess, and Q.-Z. Yin (2011), The lunar magma ocean: Reconciling the solidification process with lunar petrology and geochronology, *Earth Planet. Sci. Lett.*, *304*, 326–336, doi:10.1016/j.epsl.2011.02.004.

Grieve, R. A. F., D. Stöffler, and A. Deutsch (1991), The Sudbury structure: Controversial or misunderstood?, *J. Geophys. Res.*, *96*, 22,753–22,764, doi:10.1029/91JE02513.

Harris, A. J. L., and J. S. Allen (2008), One-, two- and three-phase viscosity treatments for basaltic lava flows, *J. Geophys. Res.*, *113*, B09212, doi:10.1029/2007JB005035.

Hartmann, W. K. (1980), Dropping stones in magma oceans: Effects of early lunar cratering, in *Proceedings of the Conference on the Lunar Highlands Crust*, pp. 155–171, Pergamon Press, Elmsford, N. Y.

Head, J. W. (1974), Orientale multi-ringed basin interior and implications for the petrogenesis of lunar highland samples, *Moon*, *11*, 327–356, doi:10.1007/BF00589168.

Head, J. W., S. Murchie, J. F. Mustard, C. M. Pieters, G. Neukum, A. McEwen, R. Greeley, E. Nagel, and M. J. S. Belton (1993), Lunar impact basins: New data for the western limb and far side (Orientale and South Pole-Aitken Basins) from the first Galileo flyby, *J. Geophys. Res.*, *98*, 17,149–17,181, doi:10.1029/93JE01278.

Head, J. W., C. I. Fassett, S. J. Kadish, D. E. Smith, M. T. Zuber, G. A. Neumann, and E. Mazarico (2010), Global distribution of large lunar craters: Implications for resurfacing and impactor populations, *Science*, *329*, 1504–1507, doi:10.1126/science.1195050.

Howard, K. A., D. E. Wilhelms, and D. H. Scott (1974), Lunar basin formation and highland stratigraphy, *Rev. Geophys.*, *12*, 309–327, doi:10.1029/RG012i003p00309.

Hurwitz, D. M., and D. A. Kring (2014), Differentiation of the South Pole–Aitken basin impact melt sheet: Implications for lunar exploration, *J. Geophys. Res. Planets*, *119*, 1110–1133, doi:10.1002/2013JE004530.

Ivanov, B. A., H. J. Melosh, and E. Pierazzo (2010), Basin-forming impacts: Reconnaissance modeling, *Geol. Soc. Am. Spec. Pap.*, *465*, 29–49, doi:10.1130/2010.2465(03).

Marsh, B. D. (1981), On the crystallinity, probability of occurrence, and rheology of lava and magma, *Contrib. Mineral. Petrol.*, *78*, 85–98, doi:10.1007/BF00371146.

Martin, D., and R. Nokes (1988), Crystal settling in a vigorously converting magma chamber, *Nature*, *332*, 534–536, doi:10.1038/332534a0.

McCauley, J. F. (1977), Orientale and Caloris, *Phys. Earth Planet. Inter.*, *15*, 220–250, doi:10.1016/0031-9201(77)90033-4.

Melosh, H. J. (1989), *Impact Cratering: A Geologic Process*, Oxford Univ. Press, New York.

Melosh, H. J., et al. (2013), The origin of lunar mascon basins, *Science*, *340*, 1552–1555, doi:10.1126/science.1235768.

Morrison, D. A. (1998), Did a thick South Pole-Aitken basin melt sheet differentiate to form cumulates?, *Proc. Lunar Planet. Sci. Conf. 29th*, Abstract 1657.

Nemchin, A., N. Timms, R. Pidgeon, T. Geisler, S. Reddy, and C. Meyer (2009), Timing of crystallization of the lunar magma ocean constrained by the oldest zircon, *Nat. Geosci.*, *2*, 133–136, doi:10.1038/ngeo417.
O'Connell-Cooper, C. D., and J. G. Spray (2011), Geochemistry of the impact-generated melt sheet at Manicouagan: Evidence for fractional crystallization, *J. Geophys. Res.*, *116*, B06204, doi:10.1029/2010JB008084.
O'Keefe, J. D., and T. J. Ahrens (1975), Shock effects from a large impact on the Moon, *Proc. Lunar Planet. Sci. Conf. 6th*, 2831–2844.
O'Keefe, J. D., and T. J. Ahrens (1977), Impact-induced energy partitioning, melting, and vaporization on terrestrial planets, *Proc. Lunar Planet. Sci. Conf. 8th*, 3357–3374.
Onorato, P. I. K., D. R. Uhlmann, and C. H. Simonds (1978), The thermal history of the Manicouagan Impact Melt Sheet, Quebec, *J. Geophys. Res.*, *83*, 2789–2798, doi:10.1029/JB083iB06p02789.
Pieters, C. M., S. Tompkins, J. W. Head, and P. C. Hess (1997), Mineralogy of the mafic anomaly in the South Pole-Aitken basin: Implications for excavation of the lunar mantle, *Geophys. Res. Lett.*, *24*, 1903–1906, doi:10.1029/97GL01718.
Pinkerton, H., and R. J. Stevenson (1992), Methods of determining the rheological properties of magmas at sub-liquidus temperatures, *J. Volcanol. Geotherm. Res.*, *53*, 47–66, doi:10.1016/0377-0273(92)90073-M.
Roscoe, R. (1952), The viscosity of suspensions of rigid spheres, *Br. J. Appl. Phys.*, *3*, 267–269, doi:10.1088/0508-3443/3/8/306.
Ryder, G., and J. F. Bower (1977), Petrology of Apollo 15 black-and-white Rocks 15445 and 15455—Fragments of the Imbrium Impact Melt Sheet?, *Proc. Lunar Planet. Sci. Conf. 8th*, 1895–1923.
Ryder, G., and P. Spudis (1987), Chemical composition and origin of Apollo 15 impact melts, *J. Geophys. Res.*, *92*, E432–E446, doi:10.1029/JB092iB04p0E432.
Ryerson, F. J., H. C. Weed, and A. J. Piwinskii (1988), Rheology of subliquidus magmas: 1. Picritic compositions, *J. Geophys. Res.*, *93*, 3421–3436, doi:10.1029/JB093iB04p03421.
Shaw, H. R. (1969), Rheology of basalt in the melting range, *J. Petrol.*, *10*, 510–535, doi:10.1093/petrology/10.3.510.
Smrekar, S., and C. M. Pieters (1985), Near-infrared spectroscopy of probable impact melt from three large lunar highland craters, *Icarus*, *63*, 442–452, doi:10.1016/0019-1035(85)90056-9.
Spudis, P. D. (2005), *The Geology of Multi-Ring Impact Basins: The Moon and Other Planets*, Cambridge Univ. Press, Cambridge, U. K.
Spudis, P. D., D. J. P. Martin, and G. Kramer (2014), Geology and composition of the Orientale basin impact melt sheet, *J. Geophys. Res. Planets*, *119*, 19–29, doi:10.1002/2013JE004521.
Suckale, J., L. T. Elkins-Tanton, and J. A. Sethian (2012), Crystals stirred up: 2. Numerical insights into the formation of the earliest crust on the Moon, *J. Geophys. Res.*, *117*, E08005, doi:10.1029/2012JE004067.
Taylor, G. J., P. H. Warren, G. Ryder, J. Delano, C. M. Pieters, and G. Lofgren (1991), Lunar rocks, in *Lunar Sourcebook*, pp. 183–284, Cambridge Univ. Press, Cambridge, U. K.
Vaughan, W. M., and J. W. Head (2014), Impact melt differentiation in the South Pole-Aitken basin: Some observations and speculations, *Planet. Space Sci.*, *91*, 101–106, doi:10.1016/j.pss.2013.11.010.
Vaughan, W. M., J. W. Head, L. Wilson, and P. C. Hess (2013), Geology and petrology of enormous volumes of impact melt on the Moon: A case study of the Orientale basin impact melt sea, *Icarus*, *223*, 749–765, doi:10.1016/j.icarus.2013.01.017.
Walker, D., J. Longhi, and J. F. Hays (1975), Differentiation of a very thick magma body and implications for the source regions of mare basalts, *Proc. Lunar Planet. Sci. Conf. 6th*, 1103–1120.
Warren, P. H. (1985), The magma ocean concept and lunar evolution, *Annu. Rev. Earth Planet. Sci.*, *13*, 201–240.
Warren, P. H., P. Clayes, and E. Cedillo-Pardo (1996), Mega-impact melt petrology (Chicxulub, Sudbury, and the Moon): Effects of scale and other factors on potential for fractional crystallization and development of cumulates, *Geol. Soc. Am. Spec. Pap.*, *307*, 105–124.
Warren, P. H., F. Ulff-Møller, and G. W. Kallemeyn (2005), "New" lunar meteorites: Impact melt and regolith breccias and large-scale heterogeneities of the upper lunar crust, *Meteorit. Planet. Sci.*, *40*, 989–1014, doi:10.1111/j.1945-5100.2005.tb00169.x.
Weill, D. F., R. A. F. Grieve, I. S. McCallum, and Y. Bottinga (1971), Mineralogy-petrology of lunar samples. Microprobe studies of samples 12021 and 12022; viscosity of melts of selected lunar compositions, *Proc. Lunar Planet. Sci. Conf. 1st*, 413–430.
Whitehead, J., R. A. F. Grieve, and J. G. Spray (2002), Mineralogy and petrology of melt rocks from the Popigai impact structure, Siberia, *Meteorit. Planet. Sci.*, *37*, 623–647, doi:10.1111/j.1945-5100.2002.tb00844.x.
Whitten, J., J. W. Head, M. Staid, C. M. Pieters, J. Mustard, R. Clark, J. Nettles, R. L. Klima, and L. Taylor (2011), Lunar mare deposits associated with the Orientale impact basin: New insights into mineralogy, history, mode of emplacement, and relation to Orientale Basin evolution from Moon Mineralogy Mapper (M3) data from Chandrayaan-1, *J. Geophys. Res.*, *116*, E00G09, doi:10.1029/2010JE003736.
Wilhelms, D. E., F. John, and N. J. Trask (1987), The geologic history of the Moon U.S. Geol. Surv. Prof. Pap. No. 1348.
Wood, J. A. (1975), Lunar petrogenesis in a well-stirred magma ocean, *Proc. Lunar Planet. Sci. Conf. 6th*, 1087–1102.
Zieg, M. J., and B. D. Marsh (2005), The Sudbury Igneous Complex: Viscous emulsion differentiation of a superheated impact melt sheet, *Geol. Soc. Am. Bull.*, *117*, 1427–1450, doi:10.1130/B25579.1.